publish it, and Dr J. V. Sanders for comprehensive criticism of the manuscript.

References

ALLPRESS, J. G., HEWAT, E. A., MOODIE, A. F. & SANDERS, J. V. (1972). *Acta Cryst.* A**28**, 528–536.
ALLPRESS, J. G. & SANDERS, J. V. (1973). *J. Appl. Cryst.* **6**, 165–190.
ANSTIS, G. R., LYNCH, D. F., MOODIE, A. F. & O'KEEFE, M. A. (1973). *Acta Cryst.* A**29**, 138–147.
BILLINGTON, C. & KAY, N. R. (1974). *Aust. J. Phys.* **27**, 73–85.
COWLEY, J. M. & MOODIE, A. F. (1960). *Proc. Phys. Soc.* **76**, 378–384.
DOWELL, W. C. T., GOODMAN, P. & WILSON, A. (1974). *Proceedings of International Crystallography Conf., Melbourne*, pp. 308–309.
GOODMAN, P. & MOODIE, A. F. (1974). *Acta Cryst.* A**30**, 280–290.
IIJIMA, S. (1971). *J. Appl. Phys.* **42**, 5891–5893.
LYNCH, D. F. & O'KEEFE, M. A. (1972). *Acta Cryst.* A**28**, 536–548.
LYNCH, D. F., MOODIE, A. F. & O'KEEFE, M. A. (1974). *Proceedings of Eighth International Congress on Electron Microscopy, Canberra*, Vol. 1, pp. 222–223.
MOODIE, A. F. (1972). *Z. Naturforsch.* **27**a, 437–440.
MOODIE, A. F. (1975). To be published.
O'KEEFE, M. A. (1973). *Acta Cryst.* A**29**, 389–401.
O'KEEFE, M. A. & SANDERS, J. V. (1975). *Acta Cryst.* A**31**, 307–310.
SCHERZER, O. (1949). *J. Appl. Phys.* **20**, 20–29.

Acta Cryst. (1975). A**31**, 307

n-Beam Lattice Images. VI. Degradation of Image Resolution by a Combination of Incident-Beam Divergence and Spherical Aberration

BY M. A. O'KEEFE AND J. V. SANDERS

CSIRO Division of Tribophysics, University of Melbourne, Parkville, Victoria 3052, *Australia*

(*Received* 5 *November* 1974; *accepted* 20 *December* 1974)

Lattice images were computed with increasing incident-beam divergence with spherical aberration taken into account. The effect is as if the outer diffracted beams transmitted by the objective aperture do not contribute to the image, so that the resolution is effectively less than that expected from the aperture size. Images of $Nb_{12}O_{29}$, calculated with the inclusion of this effect, show improved agreement with experimental images.

1. Introduction

An electron microscope without aberrations would give a lattice image of great detail and contrast, which could be simply interpreted if the specimen were thin enough. The most important aberration is, of course, spherical aberration of the objective lens, and its effect on the image is generally reduced by inserting an objective aperture to exclude the diffracted beams whose phases are most severely modified. The aperture size is usually carefully selected to match the value of the spherical aberration coefficient (C_S) of the objective lens (Scherzer, 1949). The effects of spherical aberration and of the introduction of an objective aperture introduce complications into the interpretation of the lattice image, and these have been discussed in general in part I,* in Allpress & Sanders (1973) and in detail in part IV.* It was shown in part IV that for a thin-enough crystal, the image could be simply approximated by calculating a 'restricted, projected charge density' (*n*-PCD) image, which had a resolution determined by the number of diffracted beams, *n*, which were transmitted through the objective aperture.

Earlier in this series, the other aberrations introduced into the lattice image by the imperfections in the electron microscope were classified into two groups:

(*a*) those which modify the image, but without loss of detail; and

(*b*) 'smearing' aberrations which produce overlapping differences in detail and hence result in loss of detail; for example the energy spread of the electrons produces an indefiniteness into the position of the image plane, and hence produces the superposition of a number of different images in any selected image plane.

A consideration of the effect of these various aberrations showed that, of those of the 'smearing' type, the divergence of the incident illumination could be the most important. Two ways in which divergence influenced the image were previously considered:

(i) The amplitudes and phases of the diffracted beams depend upon the angle of incidence of the electron beam. For crystals thin enough to satisfy *n*-PCD

* Previous papers in this series are: Part I – Allpress, Hewat, Moodie & Sanders (1972). Part II – Lynch & O'Keefe (1972). Part III – Anstis, Lynch, Moodie & O'Keefe (1973). Part IV – O'Keefe (1973). Part V – Lynch, Moodie & O'Keefe (1975).

conditions this effect was found to be quite small for the values of divergence used in practice.

(ii) In defocused images the divergence of each non-axial ray introduces a translation of image points which increases with amount of defocus, and with increase in the angle of deviation of the incident ray from the axial one. Any point in the defocused image therefore contains contributions from different image points within the range of divergence, and the final image consists of the superposition of all these images. This effect was found to be important for images more than 0·1 μm out of focus, when resolutions of about 3 Å are involved.

We consider in this paper a third consequence of the divergence which does not seem to have been considered in detail previously, and which is found to be most important in limiting the resolution *in general* in images formed predominantly by phase contrast of transmitted 100 kV electrons. This aberration is a result of the variation in phase introduced across the cone of each divergent diffracted beam by the spherical aberration, so that the contributions of those outer beams transmitted through the objective aperture are effectively nullified in the resultant image.

2. Calculation

Under the illuminating conditions used to record lattice images, each diffracted beam appears as a disc in the diffraction pattern. A typical example in Fig. 1 shows the part of the diffraction pattern from $Nb_{12}O_{29}$ transmitted through the objective aperture, whose image is the limiting circle (radius equivalent to $1{\cdot}2\times10^{-2}$ rad) in the figure. The size of each disc is determined by the divergence of the incident illumination (half-angle of cone is $1{\cdot}4\times10^{-3}$ rad in this case), and the angle of incidence onto the crystal varies across this disc. The problem is to compute the separate contributions from all these beams of varying angle of incidence, and sum them in the final image. If coherence exists across the disc, the amplitudes and phases should be summed. However, no interference effects (fringes) in overlapping areas of discs have been observed in these diffraction patterns. The components are therefore considered to be completely or partially incoherent, and intensities were added in the final sum.

A number of problems arise in computing the wave field due to non-normal incidence, and three different situations can be considered (Fig. 2).

In general, the non-aberrated propagator is

$$P(h,k)=\exp\{-i\pi R\lambda(u^2+v^2)\}$$

where u,v are reciprocal-space coordinates (Cowley & Moodie, 1960).

For propagation through distance R within the crystal (multislice calculation), this may be written as

$$P_R(h,k)=\exp\{2\pi i\zeta_{hk}\,.\,R\} \qquad (1)$$

where ζ_{hk} is the excitation error for the hkth reflexion.

For propagation from the exit surface of the crystal to the object plane of the lens, the propagator may be written

$$P_\varepsilon(h,k)=\exp\{2\pi i\eta_{hk}\,.\,\varepsilon\} \qquad (2)$$

for an object plane distance ε from the exit surface, where η_{hk} is the (reciprocal-space) distance from the spherical wavefront to the object plane.

In considering P, three directions are important:

(i) The projection direction within the crystal (*i.e.* the normal to the slices used in multislicing).

(ii) The direction of the incident beam.

(iii) The direction of the optic axis of the objective lens.

When all three are parallel, the η_{hk} of equation (2) are numerically identical to the ζ_{hk} of (1) [Fig. 2(*a*)].

When the crystal is tilted, the ζ_{hk} of (1) change and thus the η_{hk} are no longer numerically identical to the crystal ζ_{hk} [Fig. 2(*b*)] but *are* to the untilted crystal ζ_{hk}. [In fact, for a small crystal tilt

$$\eta(h,k)\simeq\zeta(h,k)-\lambda\left\{\frac{hq}{a^2}+\frac{kr}{b^2}\right\}$$

for orthogonal axes, where (q,r) are the coordinates of the centre of the Laue circle.]

When the incident beam direction is tilted and the slice normal is parallel to the optic axis, the ζ_{hk} and η_{hk} are again numerically equivalent [Fig. 2(*c*)].

In parts I, II and IV of this series of publications, the unaberrated propagator external to the crystal was given as $P_\varepsilon=\exp(2\pi i\zeta_{hk}\,.\,\varepsilon)$. This is numerically correct (if notationally inaccurate) for the situation considered in parts I and II where only those reflexions lying on a systematics line were considered [equivalent to Fig. 2(*a*)] and for the zone-axis images in part IV, but not for the tilted-crystal case of part IV where off-systematics reflexions were considered [Fig. 11(*a*) of part IV]. In this latter case, the use of ζ_{hk} instead of the correct η_{hk} produced images which were displaced *along* the main fringes, *e.g.* the darker parts of the fringes in the $\varepsilon=-20$ nm image of Fig. 11(*a*) of part IV are shown as appearing at the positions of the tetrahedral sites in $W_4Nb_{26}O_{77}$ but would be displaced a distance proportional to ε in a correct calculation.

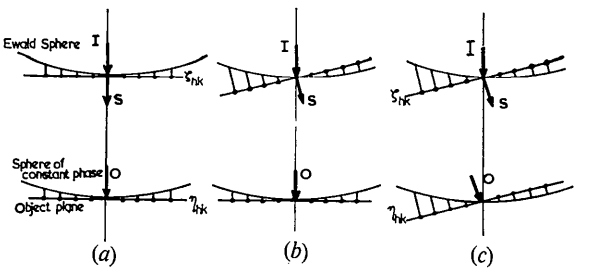

Fig. 2. Three possible (bright-field) imaging situations in the electron microscope: (*a*) Normal to crystal surface (*S*), incident electron beam (*I*) and objective lens optic axis (*O*) all parallel. (*b*) Tilted crystal. (*c*) Tilted incident beam.

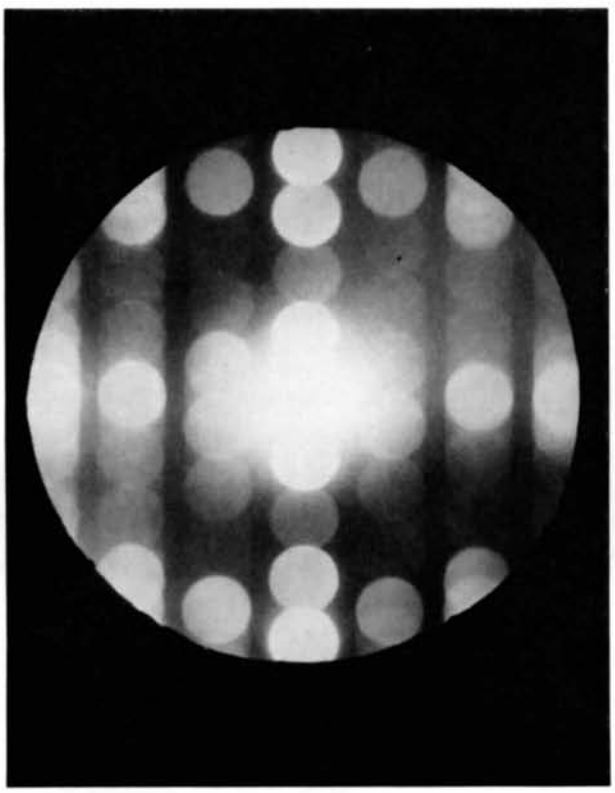

Fig. 1. *h*0*l*-zone diffraction pattern of $Nb_{12}O_{29}$ taken under imaging conditions with the field limited by the objective aperture (Courtesy of S. Iijima).

[*To face p.* 308

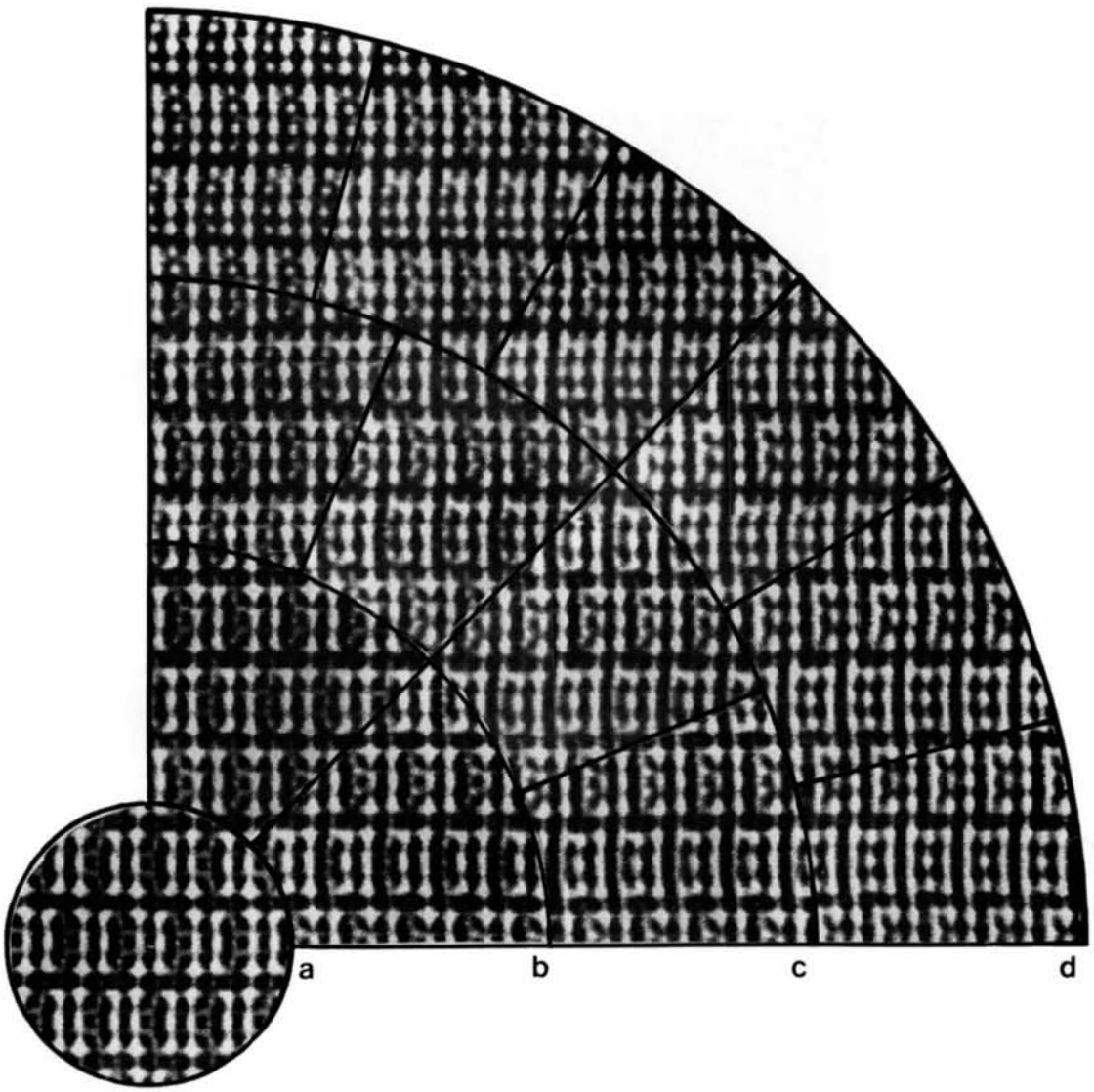

Fig. 4. n-beam lattice images calculated for the 13 angles of one quadrant of Fig. 3(b). In each case crystal thickness, $H = 50$ Å; number of beams, $n = 79$; $C_S = 1{\cdot}8$ mm; and defocus, $\varepsilon = -600$ Å.

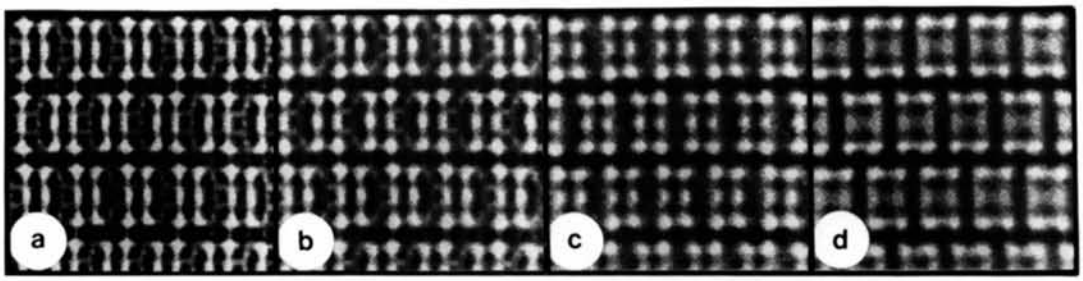

Fig. 5. Progressive degradation of resolution as the incident beam divergence is increased. (*a*) Zero divergence. (*b*) Cone half-angle of 6×10^{-4} rad. (*c*) Cone half-angle of 1×10^{-3} rad. (*d*) Experimental divergence of $1{\cdot}4\times10^{-3}$ rad, corresponding to Fig. 1.

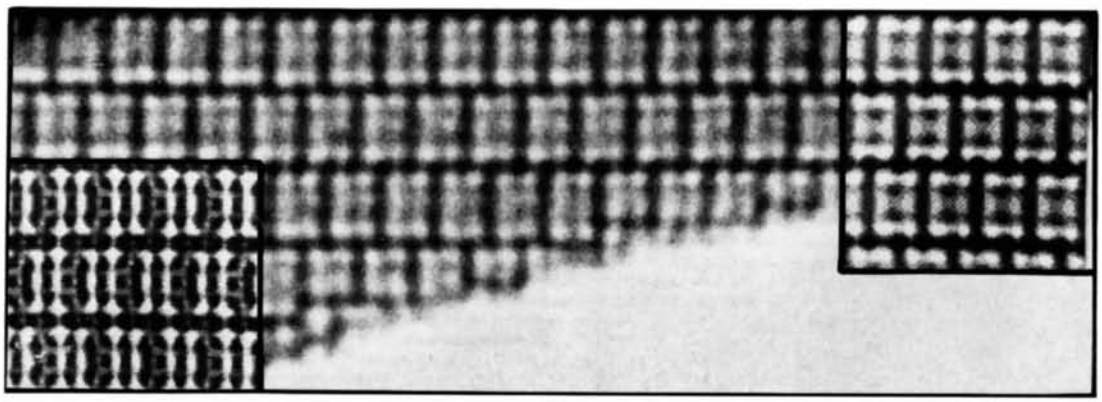

Fig. 6. Experimental image of $Nb_{12}O_{29}$ taken under the conditions of Fig. 1 (Courtesy S. Iijima). Inserts: – left-hand side has no correction [Fig. 5(*a*)]; – right-hand side is corrected for divergence [Fig. 5(*d*)].

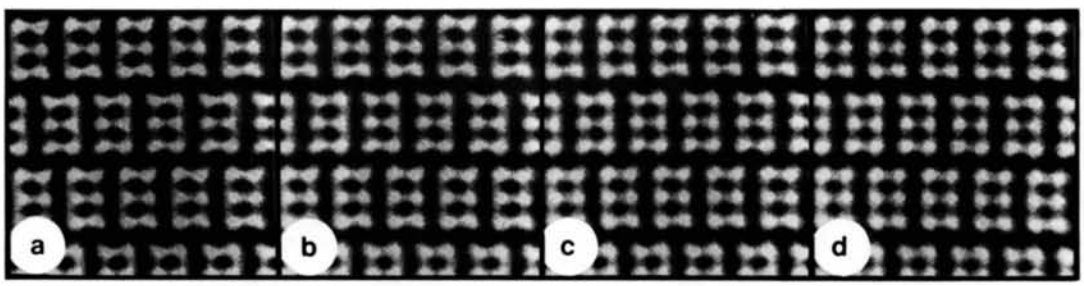

Fig. 7. Effective aperture ($n=59$ beams) images show little change with increasing divergence. (*a*) Zero divergence. (*b*) 6×10^{-4} rad. (*c*) 1×10^{-3} rad. (*d*) $1{\cdot}4\times10^{-3}$ rad.

For the present calculation, the situation shown in Fig. 2(*c*) is appropriate and the aberrated propagator $P_{\varepsilon,c_s}=\exp\{2\pi i\eta_{hk}(\varepsilon-\lambda C_s\eta_{hk})\}$ was used with the η_{hk} numerically identical with the ζ_{hk} used in the multislice calculation. The aperture was considered to transmit 79 complete diffraction discs [Fig. 3(*a*)].

3. Results

Each of the 79 diffraction spots used in the image calculation [Fig. 3(*a*)] was divided into 49 equal-area regions and a multislice (Goodman & Moodie, 1974) and image calculation (parts II and IV) carried out for the *h*0*l* zone of $Nb_{12}O_{29}$ at the angle corresponding to the centroid of each region [Fig. 3(*b*)]. The coefficient C_s was set at 1·8 mm, the experimental value for the electron microscope used in Figs. 1 and 6.

By symmetry, only 13 independent images are required (one quadrant of each diffraction spot) and these are displayed in Fig. 4. The change in character between adjacent images is small, but between the central (zero-tilt) image and those in the outermost annulus the change is quite marked. Since the images were calculated at points in concentric rings about the zero-tilt image, summations over the inner nine (out to *b* in Fig. 4) or 25 (out to *c*) images produce summed images corresponding to $\frac{3}{7}$ (half-angle of cone 6×10^{-4} rad) and $\frac{5}{7}$ (10^{-3} rad) of the experimental beam divergence. Fig. 5 shows how the image resolution is degraded by increasing divergence; steps (*a*) to (*d*) correspond to the increasing divergence produced by summing images over the discs (i) to (iv) in Fig. 3(*b*).

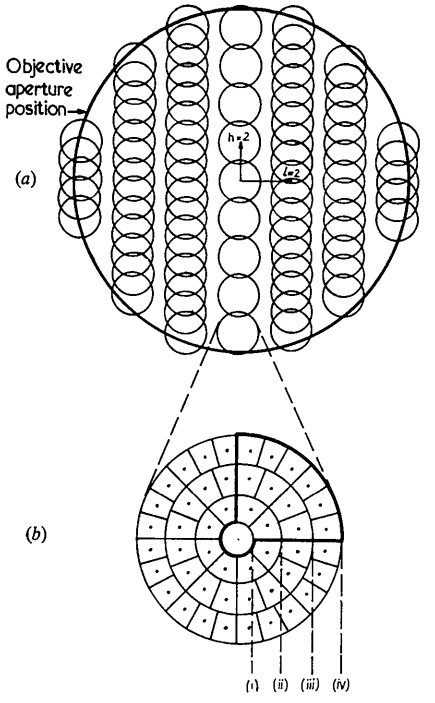

Fig. 3. Diffraction model used in the image calculation. (*a*) Showing the 79 spots used to approximate the experimental conditions shown in Fig. 1. Each spot was considered to be completely transmitted by the aperture, *i.e.* the areas cut off the peripheral spots by the aperture were considered as being transmitted. (*b*) Each diffraction spot was divided into 49 equal areas and images calculated for the angle corresponding to the centroid of each area marked by a dot. Discs (i) to (iv) indicate the magnitudes of the divergences used in image calculations.

The final image [Fig. 5(*d*)] formed by summing over the experimental divergence with the number of transmitted beams matched to experiment, is barely distinguishable from an experimental image of $Nb_{12}O_{29}$ (Fig. 6) selected from a through-focal series obtained by Iijima during an investigation of $Ti_2Nb_{10}O_{29}$ (Iijima, 1971). Note that the central pair in each group of six white spots is now blurred, just as in the experimental image.

The smearing introduced by this divergence/spherical-aberration effect reduces the resolution to that given by a much smaller objective aperture. A set of images was computed, without taking account of divergence, at small, increasing steps of resolution [d_R, defined as in IV, O'Keefe (1973), *i.e.* the distance corresponding to the highest-order reflexion transmitted through the objective aperture, and ignoring the numerical factor corresponding to the Rayleigh condition] in the range $4{\cdot}75\geq d_R\geq3{\cdot}32$ Å (corresponding to $39\leq n\leq79$), and compared carefully with those from experiment. At $d_R=3{\cdot}56$ ($n=61$) there was detail in the computed image, which became clearer at $d_R=3{\cdot}48$ and 3·42 Å (corresponding to $n=65$ and 67) and which was not apparent in the experimental, nor in the image corrected for divergence/spherical aberration.

We conclude that the experimental and the corrected images are similar to that for an aperture transmitting only 59 beams, rather than 79, that is, that the resolution is in fact only $d_R=3{\cdot}8$ Å instead of 3·3 Å as expected from the experimental aperture size. If in fact this smaller aperture had been used, then, as shown in Fig. 7, the spherical aberration/divergence is no longer important; differences between the four images corresponding to increasing divergence are nearly indistinguishable.

4. Discussion

The object of this series of papers has been to enquire into the conditions under which lattice images, obtained in a practical electron microscope can be naively interpreted as showing the structure of crystals. It has been established that for thin enough crystals (and ignoring incident-beam divergence) it is valid to use such an interpretation in terms of the projected charge-density distribution (part V), in which the resolution is restricted only by the size of the objective aperture, *i.e.* by the limited number of beams contributing to the phase-contrast image. It has been shown here that some of this detail, may, in practice, be lost by a smearing due to the combination of objective lens spherical aberration and divergence of the incident il-

lumination, so that the resolution in the image is worse than that expected for the aperture size used. These binary oxides of tungsten and niobium, having some quite intense diffraction spots near the periphery of the objective aperture, are rather sensitive to the effect. However, such beams will always be the ones contributing the finer detail in images and, therefore, the effect will always limit resolution to values more than those expected for the size of objective aperture.

The computations show how a decrease in divergence restores the lost detail. We believe that this effect is general, and that the obvious step to improved resolution, apart from reducing the value of C_S, is to improve the illuminating system of the microscope to give less divergence without loss of intensity. Fig. 5 shows that to obtain the resolution appropriate to the size of the objective aperture, the divergence should be at most half that used in our experiment, corresponding to the image in Fig. 5(*b*); much detail is still lost in Fig. 5(*c*), where the divergence is reduced by $\frac{2}{7}$.

We wish to thank Dr S. Iijima for providing the electron diffraction pattern and micrograph used in Figs. 1 and 6, and for permission to publish these. Thanks are also due to the members of the Electron Diffraction Section of the CSIRO Division of Chemical Physics, in particular to Dr D. F. Lynch and Mr A. F. Moodie for their theoretical assistance.

References

ALLPRESS, J. G., HEWAT, E. A., MOODIE, A. F. & SANDERS, J. V. (1972). *Acta Cryst.* A**28**, 528–536.
ALLPRESS, J. G. & SANDERS, J. V. (1973). *J. Appl. Cryst.* **6**, 165–190.
ANSTIS, G. R., LYNCH, D. F., MOODIE, A. F. & O'KEEFE, M. A. (1973). *Acta Cryst.* A**29**, 138–147.
COWLEY, J. & MOODIE, A. F. (1960). *Proc. Phys. Soc.* **76**, 378–384.
GOODMAN, P. & MOODIE, A. F. (1974). *Acta Cryst.* A**30**, 280–290.
IIJIMA, S. (1971). *J. Appl. Phys.* **42**, 5891–5893.
LYNCH, D. F., MOODIE, A. F. & O'KEEFE, M. A. (1975). *Acta Cryst.* A**31**, 300–307.
LYNCH, D. F. & O'KEEFE, M. A. (1972). *Acta Cryst.* A**28**, 536–548.
O'KEEFE, M. A. (1973). *Acta Cryst.* A**29**, 389–401.
SCHERZER, O. (1949). *J. Appl. Phys.* **20**, 20–29.

Acta Cryst. (1975). A**31**, 310

Probability Distribution Connected with Structure Amplitudes of Two Related Crystals. VII. The Case of an Approximately Centrosymmetric Structure*

BY P. SWAMINATHAN AND R. SRINIVASAN†

Centre of Advanced Study in Physics, University of Madras, Guindy Campus, Madras-600025, *India*

(*Received* 12 *November* 1974; *accepted* 29 *November* 1974)

The probability distribution of the structure factors F_N and F_N^c where the former refers to the 'true structure' containing N atoms at locations $\mathbf{r}_{Nj}$ and the latter to the assumed model' with N atoms at locations $\mathbf{r}_{Nj}^c$, is worked out for the situation where the assumed model is exactly centrosymmetric and the true model is approximately centrosymmetric. Other statistical distributions connected with these, such as difference, quotient, reciprocal quotient and the phase-angle difference have also been derived. Also a Booth type of discrepancy index is worked out for such a situation. Theoretical results are verified with a hypothetical model.

Introduction

In the ealier parts of the series (Part I: Ramachandran, Srinivasan & Raghupathy Sarma, 1963; Part II: Srinivasan, Raghupathy Sarma & Ramachandran, 1963*a*; Part III: Srinivasan, Subramanian & Ramachandran, 1964; Part IV: Srinivasan & Ramachandran, 1965*a*; Part V: Srinivasan & Ramachandran, 1965*b*; Part VI: Srinivasan & Ramachandran, 1966; see also, Srinivasan, Raghupathy Sarma & Ramachandran, 1963*b*; Srinivasan & Chandrasekaran, 1966 – hereafter referred to as SC; Parthasarathy & Srinivasan, 1967 – hereafter referred to as PS) the probability distributions of a pair of structure factors were considered. The results led to various statistical tests such as tests for isomorphism between a pair of crystals, and discrepancy indices for use in crystal structure analysis. The basic problem considered may be stated as the probability distribution of the structure factor of the 'true' structure containing N atoms at locations $\mathbf{r}_{Nj}$ and another 'assumed model' containing a part P of the atoms ($P \leq N$) with coordinate errors. The probability distribution function of the structure factors F_N and F_P^c, where F_N corresponds to the true structure

* Contribution No. 390 from the Centre of Advanced Study in Physics, University of Madras, Guindy Campus, Madras-600025, India.

† To whom correspondence should be addressed.